

New physics in $B \rightarrow K^* \tau^+ \tau^-$: A model independent analysis

Neetu Raj Singh Chundawat^{*}

Indian Institute of Technology Jodhpur, Jodhpur 342037, India

 (Received 16 December 2022; accepted 20 February 2023; published 6 March 2023)

In this work, we consider the implications of current $b \rightarrow s \ell^+ \ell^-$ ($\ell = e, \mu$) measurements on several $B \rightarrow K^* \tau^+ \tau^-$ observables under the assumption that the possible new physics can have both universal as well as nonuniversal couplings to leptons. For new physics solutions which provide a good fit to all $b \rightarrow s \ell^+ \ell^-$ data, we intend to identify observables with large deviations from the Standard Model (SM) predictions as well as to discriminate between various new physics solutions. For this we consider the $B \rightarrow K^* \tau^+ \tau^-$ branching fraction, the K^* longitudinal fraction f_L , the tau forward-backward asymmetry A_{FB} and the optimized observables in the $P_i^{(\prime)}$ basis. Further, we construct the $\tau - \mu$ lepton-flavor differences ($Q^{\tau\mu}$) between these tau observables and their muonic counterparts in $B \rightarrow K^* \mu^+ \mu^-$ decay. Moreover, we also consider lepton-flavor ratios ($R^{\tau\mu}$) of all of these observables. We find that the current data allows for deviations ranging from 25% up to an order of magnitude from the SM value in a number of observables. For e.g., the magnitudes of $Q_{P_3}^{\tau\mu}$ and $Q_{P_8}^{\tau\mu}$ observables can be enhanced up to an order of magnitude, a twofold enhancement in $Q_{A_{\text{FB}}}^{\tau\mu}$ is possible along with $\sim 50\%$ enhancement in $R_{K^*}^{\tau\mu}$ and $\sim 25\%$ in $R_{A_{\text{FB}}}^{\tau\mu}$. Moreover, the branching ratio of $B \rightarrow K^* \tau^+ \tau^-$ can be suppressed up to 25%. A precise measurement of these observables can also discriminate between a number of new physics solutions.

DOI: [10.1103/PhysRevD.107.055004](https://doi.org/10.1103/PhysRevD.107.055004)

I. INTRODUCTION

The measurements of several observables in decays induced by the quark level transition $b \rightarrow s \ell^+ \ell^-$ ($\ell = e, \mu$) show propitious signatures of new physics beyond the Standard Model (SM) interactions [1]. These observables are mainly related to $B \rightarrow K^* \mu^+ \mu^-$ and $B_s \rightarrow \phi \mu^+ \mu^-$ decay modes. The measured value of the optimized angular observable P_5' in $B \rightarrow K^* \mu^+ \mu^-$ in $4.0 \text{ GeV}^2 \leq q^2 \leq 6.0 \text{ GeV}^2$ bin deviates from the SM prediction at the level of 3σ [2–5]. Further, the experimental value of the branching ratio of $B_s \rightarrow \phi \mu^+ \mu^-$ decay does not concur with the SM prediction at the level of 3.5σ level [6,7]. Moreover, there is dissimilitude in the measured and SM prediction of the branching ratio $B_s \rightarrow \mu^+ \mu^-$ decay [8–13]. However, the recent measurement by the CMS Collaboration using the full Run 2 dataset [14] shifts the world average of the branching ratio $B_s \rightarrow \mu^+ \mu^-$ [15] to a value which is in excellent agreement with its SM prediction [16,17]. These disparities

can be accommodated by assuming new physics with imperative couplings to muons.

The mismatch between the electron and muon sector, owing to new physics beyond the SM, can be delineated by the ratio observables R . These observables enmesh agglomeration between different lepton flavors. The lepton-flavor universality violating (LFUV) ratios $R_K \equiv \Gamma(B^+ \rightarrow K^+ \mu^+ \mu^-) / \Gamma(B^+ \rightarrow K^+ e^+ e^-)$ and $R_{K^*} \equiv \Gamma(B^0 \rightarrow K^{*0} \mu^+ \mu^-) / \Gamma(B^0 \rightarrow K^{*0} e^+ e^-)$ has been measured by the LHCb Collaboration. The measurement of R_K showed an exiguous of 3.1σ as compared to the SM value ≈ 1 [18,19] in the $1.1 \text{ GeV}^2 \leq q^2 \leq 6.0 \text{ GeV}^2$ bin [20]. The measurements of R_{K^*} , in the $0.045 \text{ GeV}^2 \leq q^2 \leq 1.1 \text{ GeV}^2$ and $1.1 \text{ GeV}^2 \leq q^2 \leq 6.0 \text{ GeV}^2$ bins also had dissent with the SM at level of $\sim 2.5\sigma$ [21]. These anomalous measurements required new physics with nonuniversal couplings to muons and electrons.

The deviation of 3.1σ was obtained assuming $R_K^{\text{SM}} \approx 1$ which is valid only under the approximation of neglecting the QED corrections. These corrections can be significant as the lepton masses break lepton-flavor universality (LFU) and their scales are different from that of b mass scale. However in [22–24] it was shown that these corrections are small. In particular the hard-collinear logs are absent in the structure-dependent QED corrections. Hence, R_K can be

^{*}chundawat.1@iitj.ac.in

Published by the American Physical Society under the terms of the [Creative Commons Attribution 4.0 International license](https://creativecommons.org/licenses/by/4.0/). Further distribution of this work must maintain attribution to the author(s) and the published article's title, journal citation, and DOI. Funded by SCOAP³.

considered as a clean theoretical observable. The same conclusion applies to the R_{K^*} observable.

A few more lepton-flavor universality violation (LFUV) ratios have been measured by the LHCb Collaboration. These are in $B^0 \rightarrow K_S \mu^+ \mu^-$ and $B^+ \rightarrow K^{*+} \mu^+ \mu^-$ decay modes [25]. The measured values of the ratios $R_{K_S} \equiv \Gamma(B^0 \rightarrow K_S \mu^+ \mu^-) / \Gamma(B^0 \rightarrow K_S e^+ e^-)$ and $R_{K^{*+}} \equiv \Gamma(B^+ \rightarrow K^{*+} \mu^+ \mu^-) / \Gamma(B^+ \rightarrow K^{*+} e^+ e^-)$ have relatively large errors as compared to R_K and R_{K^*} and are consistent with their SM predictions below 2σ level. Apart from these ratios, the LFUV new physics can also be captured by constructing additional LFUV observables by taking difference of optimized observables in the muon and electron sector, $Q_{P_i^{(\prime)}}^{\mu e} = P_i^{(\prime)\mu} - P_i^{(\prime)e}$ [26]. The $Q_{P_4^{\mu e}}$ and $Q_{P_5^{\mu e}}$ observables have been measured by the Belle Collaboration [27]. However, due to large errors, the measured values are consistent with the SM prediction of ≈ 0 .

The above $b \rightarrow s \ell \ell$ anomalies can be analyzed in a model independent framework using the language of effective field theory. However, there can be a number of approaches under which the global analysis of $b \rightarrow s \ell \ell$ data can be performed. The most common framework is where new physics is assumed to be present only in $b \rightarrow s \mu^+ \mu^-$ decay [13,28–40]. In another approach, new physics is allowed to be present in electron sector along with muons with nonequal Wilson coefficients (WCs) [36,41,42]. Thus in both of these approaches, the new physics couplings are nonuniversal in nature.

In [43] a new approach was explored where apart from having nonuniversal WCs affecting only $b \rightarrow s \mu^+ \mu^-$ decay, one can also have universal WCs equally affecting all $b \rightarrow s \ell \ell$ processes, $\ell = e, \mu, \tau$. Although LFUV new physics contributions are mandatory to explain $R_{K^{(*)}}$ anomalies, a universal new physics contribution which is the same for all leptons is not ruled out even though measurements in $b \rightarrow s e e$ sector are consistent with SM predictions. In fact, such a contribution gives rise to scenarios with a statistical significance at least as relevant as that of only LFUV framework and can also motivate the construction of new

models beyond SM including not only LFUV but also LFU new physics contributions [35,43,44].

Very recently, on December 20, 2022, the LHCb Collaboration updated the measurements of R_K and R_{K^*} [45,46] by including the experimental systematic effects which were absent in the previous analysis. The updated measurements of R_K and R_{K^*} are now consistent with the SM predictions. A global analysis of $b \rightarrow s \ell \ell$ data using the updated measurements was performed in [47].

If both universal and nonuniversal new physics WCs are present then the universal couplings will generate new physics effects in $b \rightarrow s \tau^+ \tau^-$ decay with WCs in μ and τ sectors being the same. Therefore, it is interesting to see what impact the universal coupling determined by the updated $b \rightarrow s \ell^+ \ell^-$ ($\ell = e, \mu$) data will have on observables in decays induced by the quark level transition $b \rightarrow s \tau^+ \tau^-$. In this work we study this implication for several CP -conserving observables in $B \rightarrow K^* \tau^+ \tau^-$.¹ Apart from analysing the branching ratio, the K^* polarization fraction, the τ forward-backward asymmetry and optimized angular observables in $B \rightarrow K^* \tau^+ \tau^-$ decay, we also consider $\tau - \mu$ lepton-flavor differences ($Q^{\tau\mu}$) and ratios ($R^{\tau\mu}$) of these observables.

The plan of the work is as follows. In the next section, we discuss the fit results based on the assumption that both universal and nonuniversal coupling to leptons are present. In Sec. III we provide definitions and theoretical expressions of observables related to $B \rightarrow K^* \tau^+ \tau^-$ decay used in our analysis. In Sec. IV we provide results obtained in our work. We finally conclude in Sec. V.

II. NEW PHYSICS IN $b \rightarrow s \mu^+ \mu^-$: LFU CONSERVING AND VIOLATING APPROACH

In this section we discuss constraints on new physics couplings under the assumption that LFU new physics is allowed in addition to LFUV new physics contributions affecting only $b \rightarrow s \mu^+ \mu^-$ transition. Within the SM, the effective Hamiltonian for $b \rightarrow s \ell^+ \ell^-$ transition can be written as

$$\begin{aligned} \mathcal{H}_{\text{eff}}^{\text{SM}} = & -\frac{\alpha_{em} G_F}{\sqrt{2}\pi} V_{ts}^* V_{tb} \left[2 \frac{C_7^{\text{eff}}}{q^2} [\bar{s} \sigma^{\mu\nu} q_\nu (m_s P_L + m_b P_R) b] \bar{\ell} \gamma_\mu \ell + C_9^{\text{eff}} (\bar{s} \gamma^\mu P_L b) (\bar{\ell} \gamma_\mu \ell) \right. \\ & \left. + C_{10} (\bar{s} \gamma^\mu P_L b) (\bar{\ell} \gamma_\mu \gamma_5 \ell) \right] + \text{H.c.}, \end{aligned} \quad (1)$$

where α_{em} is the fine-structure constant, G_F is the Fermi constant, V_{ts} and V_{tb} are the Cabibbo-Kobayashi-Maskawa

¹A few examples of correlating current B anomalies with new physics in $b \rightarrow s \tau^+ \tau^-$ in specific model dependent scenarios can be seen in [48–51].

(CKM) matrix elements and $P_{L,R} = (1 \mp \gamma_5)/2$ are the chiral projection operators. The q in the C_7 term is the momentum of the off shell photon in the effective $b \rightarrow s \gamma^*$ transition.

Assuming new physics in the form of vector and axial-vector operators, the new physics effective Hamiltonian for $b \rightarrow s \ell^+ \ell^-$ process can be written as

$$\begin{aligned}
\mathcal{H}_{\text{eff}}^{\text{NP}} = & -\frac{\alpha_{\text{em}} G_F}{\sqrt{2}\pi} V_{ts}^* V_{tb} [C_{9\ell}(\bar{s}\gamma^\mu P_L b)(\bar{\ell}\gamma_\mu \ell) \\
& + C_{10\ell}(\bar{s}\gamma^\mu P_L b)(\bar{\ell}\gamma_\mu \gamma_5 \ell) + C'_{9\ell}(\bar{s}\gamma^\mu P_R b)(\bar{\ell}\gamma_\mu \ell) \\
& + C'_{10\ell}(\bar{s}\gamma^\mu P_R b)(\bar{\ell}\gamma_\mu \gamma_5 \ell)] + \text{H.c.} \quad (2)
\end{aligned}$$

Here $C_{(9,10)\ell}$ and $C'_{(9,10)\ell}$ are the new physics WCs. In the presence of LFU new physics, the WCs can be written as

$$\begin{aligned}
C_{(9,10)e} &= C_{(9,10)\tau} = C_{(9,10)}^U, \\
C'_{(9,10)e} &= C'_{(9,10)\tau} = C'_{(9,10)}^U, \\
C_{(9,10)\mu} &= C_{(9,10)}^U + C_{(9,10)\mu}^V, \\
C'_{(9,10)\mu} &= C'_{(9,10)}^U + C'_{(9,10)\mu}^V. \quad (3)
\end{aligned}$$

Hence the C^U and C'^U WCs contribute equally to all decays induced by the $b \rightarrow s\ell^+\ell^-$ transitions whereas C^V and C'^V contribute only to $b \rightarrow s\mu^+\mu^-$.

A global fit to all $b \rightarrow s\ell^+\ell^-$ data, i.e., LFUV observables along with $b \rightarrow s\mu^+\mu^-$ and $b \rightarrow se^+e^-$ observables, preferred new physics in $C_{9\mu}$ whereas a fit to all LFUV observables preferred $C_{9\mu} = -C_{10\mu}$ new physics scenario. Therefore a 2D scenario with C_9^U along with $C_9^V = -C_{10}^V$ is

expected to provide a good fit to data, with a significance at least at the level of fits with only LFUV contributions, if not better. This motivated a new approach in which apart from having nonuniversal WCs affecting only $b \rightarrow s\mu^+\mu^-$ decay, an universal component equally affecting all $b \rightarrow s\ell^+\ell^-$ processes, $\ell = e, \mu, \tau$ was explored [43]. Indeed such a scenario provided an extremely good fit to all $b \rightarrow s\ell^+\ell^-$ data [35]. A complete set of all such scenarios are illustrated in Table I. These scenarios can be classified into two categories:

- (i) Class-A (scenarios characterized by C_9^U contribution): Here we have four favored scenarios. These solutions were first identified in [43]. In the notation of [35] except S-V, all are 2D solutions.
- (ii) Class-B (scenarios characterized either by C_{10}^U or C_{10}^V contribution): Here again we have four favored solutions. These additional scenarios which can arise naturally in several new physics models were introduced in [44]. For e.g., S-IX can be generated in 2HDM models [52] whereas other solutions can be induced in Z' models with vectorlike quarks [53,54].

In Table I, we list the 1σ range of WCs along with pull for each favored scenarios as obtained in [35]. These values were obtained by performing a global fit to all available data except measurements related to $\Lambda_b \rightarrow \Lambda\mu\mu$. In Table I,

TABLE I. Allowed new physics solutions [35]. In our fit, the pull is defined as $\sqrt{\chi_{\text{SM}}^2 - \chi_{\text{bf}}^2}$ where χ_{bf}^2 is the χ^2 at the best-fit value in the presence of new physics and χ_{SM}^2 is the value of χ^2 in the SM. The value of χ_{SM}^2 is ≈ 217 before December 2022. This includes the measurements of R_K and R_{K^*} by the LHCb Collaboration [20,21], the measurements of R_{K^*} by the Belle Collaboration [55] and the world average of the branching ratio of $B_s \rightarrow \mu^+\mu^-$ as obtained in [13] (denoted by ‘‘old’’). In the updated fit (denoted by ‘‘new’’), using the observables listed in Sec. II, the value of χ_{SM}^2 reduces to ≈ 184 .

Solutions	WCs	1σ range [35]	Pull [35]	1σ range (old)	Pull	1σ range (new)	Pull
S-V	$C_{9\mu}^V$	(-1.02, -0.11)	6.6	(-0.98, 0.003)	7.7	(-1.31, -0.53)	4.5
	$C_{10\mu}^V$	(0.08, 0.84)		(0.15, 0.97)		(-0.66, 0.07)	
	$C_9^U = C_{10}^U$	(-0.73, 0.07)		(-0.76, 0.08)		(-0.13, 0.58)	
S-VI	$C_{9\mu}^V = -C_{10\mu}^V$	(-0.59, -0.44)	6.9	(-0.60, -0.45)	7.7	(-0.33, -0.20)	4.1
	$C_9^U = C_{10}^U$	(-0.56, -0.26)		(-0.44, -0.18)		(-0.43, -0.17)	
S-VII	$C_{9\mu}^V$	(-1.07, -0.63)	6.7	(-1.15, -0.77)	7.4	(-0.43, -0.08)	5.5
	C_9^U	(-0.52, 0.01)		(-0.35, 0.15)		(-1.07, -0.58)	
S-VIII	$C_{9\mu}^V = -C_{10\mu}^V$	(-0.41, -0.27)	7.2	(-0.47, -0.32)	7.9	(-0.18, -0.05)	5.6
	C_9^U	(-0.99, -0.63)		(-0.87, -0.45)		(-1.15, -0.77)	
S-IX	$C_{9\mu}^V = -C_{10\mu}^V$	(-0.63, -0.43)	6.3	(-0.61, -0.43)	7.4	(-0.27, -0.12)	3.6
	C_{10}^U	(-0.44, -0.05)		(-0.32, 0.07)		(-0.09, 0.27)	
S-X	$C_{9\mu}^V$	(-1.13, -0.84)	6.9	(-1.10, -0.82)	7.8	(-0.72, -0.41)	4.6
	C_{10}^U	(0.13, 0.42)		(0.19, 0.50)		(0.05, 0.34)	
S-XI	$C_{9\mu}^V$	(-1.20, -0.91)	6.9	(-1.23, -0.95)	7.8	(-0.82, -0.51)	4.6
	C_{10}^U	(-0.35, -0.10)		(-0.37, -0.16)		(-0.26, -0.04)	
S-XIII	$C_{9\mu}^V$	(-1.27, -0.96)	6.7	(-1.27, -0.98)	8.1	(-0.96, -0.60)	5.1
	$C_{9\mu}^V$	(0.13, 0.60)		(0.20, 0.59)		(0.22, 0.63)	
	C_{10}^U	(0.10, 0.47)		(0.14, 0.52)		(0.01, 0.38)	
	C_{10}^U	(-0.15, 0.21)		(-0.17, 0.14)		(-0.08, 0.24)	
	C_{10}^U						

we also provide our fit results using the methodology adopted in Refs [38] and using the updated measurements of R_K and R_{K^*} by the LHCb Collaboration in December, 2022 [45,46]. We also use the modified world average of the branching ratio of $B_s \rightarrow \mu^+\mu^-$ in the light of updated measurement from the CMS Collaboration [14,15]. In addition, we included observables from $b \rightarrow se^+e^-$ sector. For comparison, we also provide our fit results using data before December 2022 updates. In the following we list all observable used in our fit.

We include following LFUV observables in the fit: The updated measurement of R_K and R_{K^*} by the LHCb Collaboration in December 2022 using the full Run 1 and 2 dataset [45,46]. We do not include measurements of the ratios $R_{K_s^0}$ and $R_{K^{*+}}$ by the LHCb Collaboration [25] in our updated fits as they are expected to suffer from the same experimental systematic effects that lead to the updated values of R_K and R_{K^*} which are now consistent with their SM predictions. Further, we do not include $Q_{P_4}^{\mu e}$ and $Q_{P_5}^{\mu e}$ in the fits.

We now list $b \rightarrow s\mu^+\mu^-$ observables used in the fit. Here we do not include any measurements in the intermediate q^2 regions, i.e., $6 \text{ GeV}^2 \leq q^2 \leq 14.0 \text{ GeV}^2$.

- (1) The updated world average of the branching ratio of $B_s \rightarrow \mu^+\mu^-$ which is $(3.45 \pm 0.29) \times 10^{-9}$ as obtained by the HFLAV averaging group [15,47]. This updated value is due to new analysis performed by the CMS Collaboration with the full Run 2 dataset [14].
- (2) Recently updated differential branching fraction measurements of $B_s \rightarrow \phi\mu^+\mu^-$ by LHCb in various q^2 intervals [7].
- (3) The differential branching ratios of $B^0 \rightarrow K^{*0}\mu^+\mu^-$ [56–58], $B^+ \rightarrow K^{*+}\mu^+\mu^-$, $B^0 \rightarrow K^0\mu^+\mu^-$ and $B^+ \rightarrow K^+\mu^+\mu^-$ [58,59] in different q^2 bins.
- (4) The branching fraction of inclusive decay mode $B \rightarrow X_s\mu^+\mu^-$ [60] where X_s is a hadron containing only one kaon is included in the fit in the low and high- q^2 bins.
- (5) The longitudinal polarization fraction f_L , forward-backward asymmetry A_{FB} and observables S_3 , S_4 , S_5 , S_7 , S_8 , S_9 in the decay $B^0 \rightarrow K^{*0}\mu^+\mu^-$ in various intervals of q^2 , as measured by the LHCb Collaboration in 2020 [4], along with their experimental correlations.
- (6) The angular observables f_L , P_1 , P_4' , P_5' , P_6' , and P_8' in $B^0 \rightarrow K^{*0}\mu^+\mu^-$ decay measured by ATLAS [61] and P_1 , P_5' measured by CMS [62]. The measurements of f_L and A_{FB} by the CDF and CMS Collaborations are also included [57,58].
- (7) The full set of angular observables for $B^+ \rightarrow K^{*+}\mu^+\mu^-$ decay mode was determined for the first time by LHCb in 2020 [63]. Here, we consider results for f_L and $P_1 - P_8'$ optimized angular observables, along with their experimental correlation [63].
- (8) We include the CP -averaged observables f_L , S_3 , S_4 , and S_7 in $B_s \rightarrow \phi\mu^+\mu^-$ decays measured by the LHCb in 2021 with the available experimental correlations [64].

The eleven $b \rightarrow se^+e^-$ observables used in our global analysis are as follows:

- (1) The measurement of differential branching fraction of $B^0 \rightarrow K^{*0}e^+e^-$ in $0.001 \leq q^2 \leq 1.0 \text{ GeV}^2$ bin by the LHCb Collaboration [65].
- (2) The measurement of differential branching fraction of $B^+ \rightarrow K^+e^+e^-$ in $1.0 \leq q^2 \leq 6.0 \text{ GeV}^2$ bin by the LHCb Collaboration [66].
- (3) The measured values of the branching ratios of $B \rightarrow X_s e^+e^-$ by the BABAR Collaboration in both low as well as high- q^2 bins [60].
- (4) The longitudinal polarization fraction f_L in the decay $B^0 \rightarrow K^{*0}e^+e^-$ in $0.002 \leq q^2 \leq 1.12 \text{ GeV}^2$ bin as measured by the LHCb Collaboration [67].
- (5) The angular optimized observables P_4' and P_5' measured by the Belle Collaboration in $0.1 \leq q^2 \leq 4 \text{ GeV}^2$, $1.0 \leq q^2 \leq 6.0 \text{ GeV}^2$, and $14.18 \leq q^2 \leq 19.0 \text{ GeV}^2$ bins [27].

A global fit to above data is performed using CERN minimization code MINUIT [68]. The χ^2 function is defined as

$$\chi^2(C_i, C_j) = [\mathcal{O}_{\text{th}}(C_i, C_j) - \mathcal{O}_{\text{exp}}]^T \mathcal{C}^{-1} [\mathcal{O}_{\text{th}}(C_i, C_j) - \mathcal{O}_{\text{exp}}], \quad (4)$$

where $\mathcal{O}_{\text{th}}(C_i, C_j)$ are the theoretical predictions of N observables (179 after December 2022 update) used in the χ^2 fit, \mathcal{O}_{exp} are the corresponding central values of the experimental measurements and \mathcal{C} is the total covariance matrix. This $N \times N$ matrix is constructed by adding the individual theoretical and experimental covariance matrices. The experimental correlations are included for the angular observables in $B^0 \rightarrow K^{*0}\mu^+\mu^-$ [4], $B^+ \rightarrow K^{*+}\mu^+\mu^-$ [63], and $B_s \rightarrow \phi\mu^+\mu^-$ [64] whereas the theoretical covariance matrix includes form factors and power corrections uncertainties. These are computed using `flavio` [69] where the observables are preimplemented based on Refs. [70,71].

We quantify the goodness of fit by pull which is defined as $\sqrt{\chi_{\text{SM}}^2 - \chi_{\text{bf}}^2}$. Here χ_{SM}^2 is the value of χ^2 in the SM and χ_{bf}^2 is the χ^2 at the best-fit value in the presence of new physics. We see from Table I that the value of χ_{SM}^2 decreased from 217 to 184 indicating that the discrepancy of data from the SM has reduced considerably. All previously favored scenarios still remains the favored ones but with smaller values of pull. This is expected as the overall tension between the experimental measurements and SM has reduced. In the Sec. IV, we obtain predictions for $B \rightarrow K^*\tau^+\tau^-$ observables using our updated values of

WCs as given in Table I. In next section we provide a description of these observables.

III. $B \rightarrow K^* \ell^+ \ell^-$ OBSERVABLES

The angular distribution of $\overline{B^0} \rightarrow \overline{K^{*0}}(\rightarrow K^- \pi^+) \ell^+ \ell^-$ decay is completely encapsulated by four independent kinematical variables. These are traditionally chosen to be the three angles (θ_K , θ_ℓ , and ϕ) and the invariant mass

$$I(q^2, \theta_\ell, \theta_K, \phi) = I_1^s \sin^2 \theta_K + I_1^c \cos^2 \theta_K + (I_2^s \sin^2 \theta_K + I_2^c \cos^2 \theta_K) \cos 2\theta_\ell + I_3 \sin^2 \theta_K \sin^2 \theta_\ell \cos 2\phi + I_4 \sin 2\theta_K \sin 2\theta_\ell \cos \phi + I_5 \sin 2\theta_K \sin \theta_\ell \cos \phi + (I_6^s \sin^2 \theta_K + I_6^c \cos^2 \theta_K) \cos \theta_\ell + I_7 \sin 2\theta_K \sin \theta_\ell \sin \phi + I_8 \sin 2\theta_K \sin 2\theta_\ell \sin \phi + I_9 \sin^2 \theta_K \sin^2 \theta_\ell \sin 2\phi. \quad (6)$$

The twelve q^2 dependent angular coefficients $I_i^{(a)}$ [73–75] are bilinear combinations of the K^{*0} decay amplitudes which in turn are functions of WCs and the form-factors which depend on the long-distance effects. The functional dependence of the angular coefficients $I_i^{(a)}$ in terms of decay amplitudes (A_i) are given in the Appendix.

The full angular distribution of the CP -conjugated mode is given by $B^0 \rightarrow K^{*0}(\rightarrow K^+ \pi^-) \ell^+ \ell^-$

$$\frac{d^4 \bar{\Gamma}}{dq^2 d \cos \theta_\ell d \cos \theta_K d \phi} = \frac{9}{32\pi} \bar{I}(q^2, \theta_\ell, \theta_K, \phi). \quad (7)$$

For $\overline{B^0} \rightarrow \overline{K^{*0}}(\rightarrow K^- \pi^+) \ell^+ \ell^-$ decay, θ_K is the angle between the directions of kaon in the $\overline{K^{*0}}$ rest frame and the $\overline{K^{*0}}$ in the rest frame of \overline{B} . The angle θ_ℓ is between the directions of the ℓ^- in the dilepton rest frame and the dilepton in the rest frame of \overline{B} whereas the angle ϕ is the azimuthal angle between the plane containing the dilepton pair and the plane encompassing the kaon and pion from the $\overline{K^{*0}}$. For $B^0 \rightarrow K^{*0}(\rightarrow K^+ \pi^-) \ell^+ \ell^-$ decay mode, θ_K is the angle between the directions of kaon in the K^{*0} rest frame and the K^{*0} in the rest frame of B whereas the angle θ_ℓ is between the directions of the ℓ^+ in the dilepton rest frame and the dilepton in the rest frame of B . This leads to the following transformation of angular coefficients under CP [51]

$$I_{1,2,3,4,5,6}^{(a)} \Rightarrow \bar{I}_{1,2,3,4,5,6}^{(a)}, \quad I_{7,8,9}^{(a)} \Rightarrow -\bar{I}_{7,8,9}^{(a)}, \quad (8)$$

where $\bar{I}_i^{(a)}$ are the complex conjugate of $I_i^{(a)}$. Therefore, combining B^0 and $\overline{B^0}$ decays, one can construct following angular observables which depend upon the average of the distribution of the B^0 and $\overline{B^0}$ [74]

$$S_i^{(a)} = \frac{I_i^{(a)}(q^2) + \bar{I}_i^{(a)}(q^2)}{d(\Gamma + \bar{\Gamma})/dq^2}. \quad (9)$$

squared of the dilepton system [$q^2 = (p_B - p_{K^*})^2$]. In the notation of Ref. [72], the full angular decay distribution of $\overline{B^0} \rightarrow \overline{K^{*0}}(\rightarrow K^- \pi^+) \ell^+ \ell^-$ decay is given by

$$\frac{d^4 \Gamma}{dq^2 d \cos \theta_\ell d \cos \theta_K d \phi} = \frac{9}{32\pi} I(q^2, \theta_\ell, \theta_K, \phi), \quad (5)$$

where

The difference of these angular coefficients will result in corresponding CP -violating angular observables [74,76].

Several well-established observables in the decay of $B \rightarrow K^* \ell^+ \ell^-$ can be expressed in terms of angular coefficients $I_i^{(a)}$ as well as CP -averaged angular observables $S^{(a)}$:

- (i) The angular integrated differential decay rate can be written in terms of angular coefficients as

$$\begin{aligned} \frac{d\Gamma}{dq^2} &= \int d \cos \theta_\ell d \cos \theta_K d \phi \frac{d^4 \Gamma}{dq^2 d \cos \theta_K d \cos \theta_\ell d \phi} \\ &= \frac{3}{4} (2I_1^s + I_1^c) - \frac{1}{4} (2I_2^s + I_2^c). \end{aligned} \quad (10)$$

- (ii) The normalized forward-backward asymmetry can be expressed in terms of CP -averaged angular observables $S^{(a)}$ as

$$\begin{aligned} A_{\text{FB}} &= \left[\int_0^1 - \int_{-1}^1 \right] d \cos \theta_\ell \frac{d^2(\Gamma - \bar{\Gamma})}{dq^2 d \cos \theta_\ell} / \frac{d(\Gamma + \bar{\Gamma})}{dq^2} \\ &= \frac{3}{8} (2S_6^s + S_6^c). \end{aligned} \quad (11)$$

- (iii) The K^* longitudinal polarization fraction can be written in terms of $S^{(a)}$ observables as

$$f_L = -S_2^c. \quad (12)$$

The $S^{(a)}$ observables are more prone to hadronic uncertainties. One can construct optimized observables with reduced uncertainties by proper combination of f_L and $S^{(a)}$ observables. These observables have been proposed by several groups, see for e.g., [28,77–82]. A frequently used form is the set of observables given in [28,82]. A generalized and extensive analysis of angular distribution formalism can be found in Ref. [75]. In this work, for $B \rightarrow K^* \tau^+ \tau^-$ decay, we consider the following set of optimized observables $P_i^{(l)}$ defined in Ref. [28,82] and written in the basis of [3]:

$$\begin{aligned}
P_1 &= \frac{S_3}{2S_2^s}, & P_2 &= \frac{S_6^s}{8S_2^s}, & P_3 &= \frac{S_9}{4S_2^s}, \\
P'_4 &= \frac{S_4}{2\sqrt{-S_2^s S_2^c}}, & P'_5 &= \frac{S_5}{2\sqrt{-S_2^s S_2^c}}, \\
P'_6 &= \frac{S_7}{2\sqrt{-S_2^s S_2^c}}, & P'_8 &= \frac{S_8}{2\sqrt{-S_2^s S_2^c}}.
\end{aligned} \tag{13}$$

The $B \rightarrow K^* \ell^+ \ell^-$ observables suffer from hadronic uncertainties which is mainly due to form factors [70,71,83] and nonlocal contributions associated with charm-quark loops [83–89]. The form factors in the low- q^2 region are calculated using light-cone sum rules (LCSR) or light-meson distribution amplitudes whereas in the high- q^2 region, form factors are obtained from lattice computations [90,91].

IV. RESULTS AND DISCUSSIONS

In this section we provide predictions for several observables in $B \rightarrow K^* \tau^+ \tau^-$ within the SM as well as for various new physics scenarios considered in Sec. II. The aim is to look for deviations from the SM as well as to distinguish between various allowed beyond SM scenarios. The observables are classified into three categories:

- (i) τ observables.
- (ii) $\tau - \mu$ lepton-flavor differences.
- (iii) $\tau - \mu$ lepton-flavor ratios.

The τ observables include differential branching ratio of $B \rightarrow K^* \tau^+ \tau^-$, f_L and A_{FB} . We also consider the optimized angular observables $P_{1,2,3}$ and $P'_{4,5,6,8}$. From these observables, we construct the following $\tau - \mu$ lepton-flavor differences:

$$\begin{aligned}
Q_B^{\tau\mu} &= B(B \rightarrow K^* \tau^+ \tau^-) - B(B \rightarrow K^* \mu^+ \mu^-), \\
Q_{f_L}^{\tau\mu} &= f_L(B \rightarrow K^* \tau^+ \tau^-) - f_L(B \rightarrow K^* \mu^+ \mu^-), \\
Q_{A_{\text{FB}}}^{\tau\mu} &= A_{\text{FB}}(B \rightarrow K^* \tau^+ \tau^-) - A_{\text{FB}}(B \rightarrow K^* \mu^+ \mu^-), \\
Q_{P_i^{(j)}}^{\tau\mu} &= P_i^{(j)}(B \rightarrow K^* \tau^+ \tau^-) - P_i^{(j)}(B \rightarrow K^* \mu^+ \mu^-).
\end{aligned} \tag{14}$$

We also consider the following lepton-flavor ratios:

$$\begin{aligned}
R_{K^*}^{\tau\mu} &= \frac{B(B \rightarrow K^* \tau^+ \tau^-)}{B(B \rightarrow K^* \mu^+ \mu^-)}, \\
R_{A_{\text{FB}}}^{\tau\mu} &= \frac{A_{\text{FB}}(B \rightarrow K^* \tau^+ \tau^-)}{A_{\text{FB}}(B \rightarrow K^* \mu^+ \mu^-)}, \\
R_{f_L}^{\tau\mu} &= \frac{f_L(B \rightarrow K^* \tau^+ \tau^-)}{f_L(B \rightarrow K^* \mu^+ \mu^-)}, \\
R_{P_j}^{\tau\mu} &= \frac{P_j(B \rightarrow K^* \tau^+ \tau^-)}{P_j(B \rightarrow K^* \mu^+ \mu^-)}, \\
R_{P'_k}^{\tau\mu} &= \frac{P'_k(B \rightarrow K^* \tau^+ \tau^-)}{P'_k(B \rightarrow K^* \mu^+ \mu^-)},
\end{aligned} \tag{15}$$

where $j = 1, 2$ and $k = 4, 5$. Here we do not consider the following LFU ratios:

$$\begin{aligned}
R_{P_3}^{\tau\mu} &= \frac{P_3(B \rightarrow K^* \tau^+ \tau^-)}{P_3(B \rightarrow K^* \mu^+ \mu^-)}, \\
R_{P'_6}^{\tau\mu} &= \frac{P'_6(B \rightarrow K^* \tau^+ \tau^-)}{P'_6(B \rightarrow K^* \mu^+ \mu^-)}, \\
R_{P'_8}^{\tau\mu} &= \frac{P'_8(B \rightarrow K^* \tau^+ \tau^-)}{P'_8(B \rightarrow K^* \mu^+ \mu^-)}.
\end{aligned} \tag{16}$$

This is due the fact that these observables have large errors due to zero crossings in their q^2 spectra. The lepton-flavor differences and ratio observables have been studied in $\mu - e$ sector in Refs. [26,36,92–94].

For $B \rightarrow K^* \tau^+ \tau^-$ decay, the ditauon q^2 ranges from 15 GeV² to 19.2 GeV². Within this region, the form factors are computed using a combined fit to lattice and LCSR results. The predictions of the branching ratio, f_L , A_{FB} , optimized angular observables $P_{1,2,3}$ & $P'_{4,5,6,8}$ in $B \rightarrow K^* \tau^+ \tau^-$ decay along with the LFU ratio $R_{K^*}^{\tau\mu}$ are obtained using flavio [69]. We obtained the prediction of other LFU ratios defined above along with the difference observables $Q^{\tau\mu}$ by implementing them in flavio using the corresponding predefined τ and μ observables.

In the following, we provide integrated values of all considered observables in [15–19] q^2 bin, which is the only bin relevant for $B \rightarrow K^* \tau^+ \tau^-$ decay. The q^2 graphs will be shown only for those observables for which a noticeable deviation from the SM, say more than 25%, is allowed for atleast one of the new physics solutions. Further, we perform separate analysis for class-A and B solutions, i.e., we will firstly compare amongst various allowed solutions within one class and then look for possible distinction between the two classes of new physics solutions.

The predictions of integrated values of τ observables in [15–19] q^2 bin are exhibited in Table II. It is evident that the predictions for the branching ratio of $B \rightarrow K^* \tau^+ \tau^-$ for scenarios V and VI are consistent with the SM whereas the S-VII and S-VIII solutions can lead to a suppression of up to $\sim 25\%$ in the value of $B(B \rightarrow K^* \tau^+ \tau^-)$. This is also reflected from the graph of differential branching ratio which is portrayed in Fig. 1. It can be seen that the 1σ allowed region for S-VII and S-VIII do not overlap with the corresponding SM range. Further, no notable deviation is allowed for any of the class-B new physics solutions i.e., solutions characterized either by C_{10}^U or C'_{10}^U contributions.

The allowed values of longitudinal polarization fraction f_L for all solutions are consistent with the SM predictions. This includes class-B solutions as well. The same is true for A_{FB} and P_1 . The angular observable P_2 can be suppressed by $\sim 5\%$ as compared to the SM for the new physics solutions S-VII and S-VIII. The remaining scenarios do not provide any interesting features.

TABLE II. Results for the q^2 bin [15–19] GeV² in the SM as well as for several new physics scenarios for the branching fraction, the longitudinal fraction f_L , the τ forward backward asymmetry A_{FB} and the optimized observables $P_i^{(0)}$ in $B \rightarrow K^* \tau^+ \tau^-$ decay. Here $B_{\tau\tau}^{K^*} \equiv B(B \rightarrow K^* \tau^+ \tau^-)$.

Observable	SM	S-V	S-VI	S-VII	S-VIII	S-IX	S-X	S-XI	S-XIII
$(B_{\tau\tau}^{K^*}) \times 10^8$	2.41 ± 0.33	(2.34, 2.83)	(2.18, 2.32)	(1.56, 1.92)	(1.50, 1.77)	(2.33, 2.45)	(2.31, 2.40)	(2.35, 2.41)	(2.29, 2.48)
f_L	0.10 ± 0.01	(0.09, 0.10)	(0.11, 0.11)	(0.11, 0.12)	(0.11, 0.12)	(0.10, 0.10)	(0.09, 0.10)	(0.10, 0.10)	(0.09, 0.10)
A_{FB}	0.21 ± 0.02	(0.18, 0.22)	(0.22, 0.23)	(0.22, 0.23)	(0.23, 0.23)	(0.21, 0.22)	(0.20, 0.21)	(0.21, 0.22)	(0.20, 0.21)
P_1	-0.66 ± 0.05	(-0.66, -0.66)	(-0.66, -0.66)	(-0.66, -0.66)	(-0.66, -0.66)	(-0.66, -0.66)	(-0.66, -0.66)	(-0.65, -0.62)	(-0.70, -0.65)
P_2	0.72 ± 0.05	(0.71, 0.73)	(0.68, 0.71)	(0.64, 0.69)	(0.63, 0.67)	(0.72, 0.73)	(0.72, 0.73)	(0.73, 0.76)	(0.69, 0.74)
P_3	0.00 ± 0.02	(0.00, 0.00)	(0.00, 0.00)	(0.00, 0.00)	(0.00, 0.00)	(0.00, 0.00)	(0.00, 0.00)	(0.00, 0.00)	(0.00, 0.00)
P_4	-0.64 ± 0.01	(-0.64, -0.64)	(-0.64, -0.64)	(-0.64, -0.64)	(-0.64, -0.64)	(-0.64, -0.64)	(-0.64, -0.64)	(-0.64, -0.63)	(-0.65, -0.64)
P_5	-1.14 ± 0.09	(-1.16, -1.13)	(-1.13, -1.08)	(-1.10, -1.03)	(-1.07, -1.01)	(-1.15, -1.14)	(-1.15, -1.15)	(-1.21, -1.16)	(-1.17, -1.09)
P_6	0.00 ± 0.13	(0.00, 0.00)	(0.00, 0.00)	(0.00, 0.00)	(0.00, 0.00)	(0.00, 0.00)	(0.00, 0.00)	(0.00, 0.00)	(0.00, 0.00)
P_8	0.00 ± 0.02	(0.00, 0.00)	(0.00, 0.00)	(0.00, 0.00)	(0.00, 0.00)	(0.00, 0.00)	(0.00, 0.00)	(0.00, 0.00)	(0.00, 0.00)

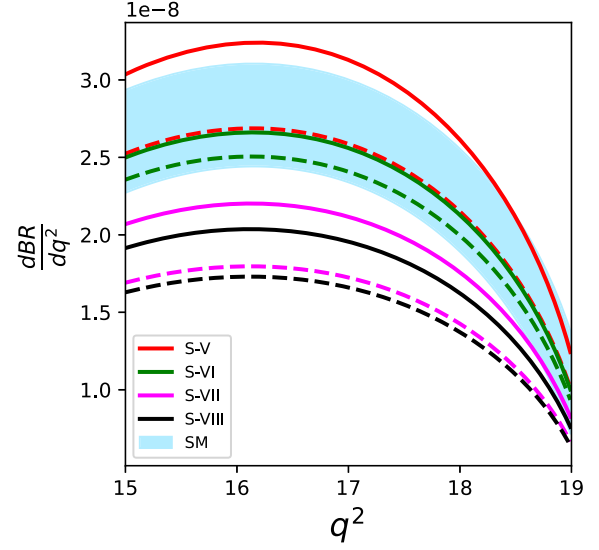


FIG. 1. Plot for the q^2 distribution in the SM as well as for class-A new physics solutions for the branching fraction of $B \rightarrow K^* \tau^+ \tau^-$. The light blue band is due to theoretical uncertainties. The thick and dotted lines represent maximum deviation from the SM for each new physics solutions. We have not shown plots for other τ observables as their predictions for all considered new physics scenarios only show marginal or negligible deviations from the SM.

The value of P_3 in SM is 0.00 ± 0.02 . As illustrated in the Table II, none of the new physics scenarios can provide any useful enhancement in the P_3 observable. The value of P_4 in the SM is ~ -0.6 which remains almost the same for all considered scenarios. The SM prediction for P_5 observable is ~ -1 . Any large deviation in this observable is forbidden by the current $b \rightarrow s \ell \ell$ data as can be seen from Table II. Within the SM, the value of observable P_6 is 0.00 ± 0.13 . All four scenarios considered in our analysis do not show any improvement over SM value as culminated from the table. For P_8 , the results are in the similar lines to that of observable P_3 .

Thus, it is evident from Table II that none of the new physics solutions considered in this work can provide a large deviation, say 50% or more, from the SM prediction in any of the τ -observables under consideration. Only a deviation of 25% is allowed in the branching ratio of $B \rightarrow K^* \tau \tau$ for S-VII and S-VIII solutions which belong to the class-A scenario. It should be noted that this deviation is in the form of suppression, i.e., the current new physics solutions can only provide suppression in the τ observables. As far as discriminating new physics solutions are concerned, the fact that deviation is not substantial, a very precise measurement would be required. None of the class-B solutions can provide any notable deviation from the SM in any of the τ observables. Therefore, any observational suppression in $B(B \rightarrow K^* \tau^+ \tau^-)$ would provide evidence in support of class-A new physics in the form of the S-VII and S-VIII solutions.

TABLE III. Results for the q^2 bin [15–19] GeV² in the SM as well as for several new physics scenarios for the $\tau - \mu$ lepton-flavor difference observables (the $Q^{\tau\mu}$ observables) for the longitudinal fraction f_L , the forward-backward asymmetry A_{FB} and the optimized observables $P_i^{(0)}$.

Observable	SM	S-V	S-VI	S-VII	S-VIII	S-IX	S-X	S-XI	S-XIII
$Q_{f_L}^{\tau\mu}$	-0.24 ± 0.02	$(-0.25, -0.23)$	$(-0.23, -0.22)$	$(-0.23, -0.22)$	$(-0.22, -0.21)$	$(-0.24, -0.24)$	$(-0.24, -0.24)$	$(-0.24, -0.24)$	$(-0.24, -0.23)$
$Q_{A_{\text{FB}}}^{\tau\mu}$	-0.15 ± 0.02	$(-0.19, -0.06)$	$(-0.14, -0.11)$	$(-0.12, -0.06)$	$(-0.11, -0.08)$	$(-0.16, -0.15)$	$(-0.16, -0.13)$	$(-0.15, -0.13)$	$(-0.20, -0.12)$
$Q_{P_1}^{\tau\mu}$	-0.037 ± 0.002	$(-0.04, -0.04)$	$(-0.04, -0.04)$	$(-0.04, -0.04)$	$(-0.04, -0.04)$	$(-0.04, -0.03)$	$(-0.04, -0.04)$	$(-0.05, -0.04)$	$(-0.14, -0.06)$
$Q_{P_2}^{\tau\mu}$	0.35 ± 0.02	$(0.35, 0.43)$	$(0.33, 0.35)$	$(0.32, 0.35)$	$(0.31, 0.33)$	$(0.35, 0.35)$	$(0.36, 0.37)$	$(0.37, 0.39)$	$(0.32, 0.38)$
$Q_{P_3}^{\tau\mu}$	0.000 ± 0.001	$(0.00, 0.00)$	$(0.00, 0.00)$	$(0.00, 0.00)$	$(0.00, 0.00)$	$(0.00, 0.00)$	$(0.00, 0.00)$	$(0.00, 0.00)$	$(-0.01, 0.00)$
$Q_{P_4}^{\tau\mu}$	-0.008 ± 0.001	$(-0.01, -0.01)$	$(-0.01, -0.01)$	$(-0.01, -0.01)$	$(-0.01, -0.01)$	$(-0.01, -0.01)$	$(-0.01, -0.01)$	$(-0.01, -0.01)$	$(-0.03, -0.01)$
$Q_{P_5}^{\tau\mu}$	-0.55 ± 0.06	$(-0.67, -0.54)$	$(-0.55, -0.53)$	$(-0.56, -0.50)$	$(-0.52, -0.49)$	$(-0.56, -0.55)$	$(-0.58, -0.56)$	$(-0.62, -0.58)$	$(-0.58, -0.47)$
$Q_{P_6}^{\tau\mu}$	0.00 ± 0.06	$(0.00, 0.00)$	$(0.00, 0.00)$	$(0.00, 0.00)$	$(0.00, 0.00)$	$(0.00, 0.00)$	$(0.00, 0.00)$	$(0.00, 0.00)$	$(0.00, 0.00)$
$Q_{P_7}^{\tau\mu}$	0.000 ± 0.001	$(0.00, 0.00)$	$(0.00, 0.00)$	$(0.00, 0.00)$	$(0.00, 0.00)$	$(0.00, 0.00)$	$(0.00, 0.00)$	$(0.00, 0.00)$	$(0.00, 0.01)$

We now consider LFU observables constructed by taking difference of observables in the decay of $B \rightarrow K^* \tau^+ \tau^-$ and $B \rightarrow K^* \mu^+ \mu^-$. These $Q^{\tau\mu}$ observables are defined in Eqs. (14). The prediction of $Q^{\tau\mu}$ observables for the q^2 bin [15–19] GeV² in the SM as well as for considered new physics scenarios are shown in Table III.

The LFU difference between the longitudinal polarization fractions, $Q_{f_L}^{\tau\mu}$, is predicted to be ~ -0.25 in the SM. This predicted value remains the same for all new physics scenarios under consideration, including class-B solutions. The observable $Q_{A_{\text{FB}}}^{\tau\mu}$ provides promising features as its value can be enhanced as compared to the SM for S-V and S-VII solutions. These solutions can provide an amelioration up to twofold in the value of $Q_{A_{\text{FB}}}^{\tau\mu}$ above its SM prediction. The same feature is also reflected in the q^2 distribution plot of $Q_{A_{\text{FB}}}^{\tau\mu}$ as shown in Fig. 2. It should be noted that none of the class-B solutions can provide any visible deviation from the SM prediction of $Q_{A_{\text{FB}}}^{\tau\mu}$. Thus any prominent deviation in this observable would disfavor class-B solutions.

We now analyze lepton-flavor differences for optimized observables. We firstly consider class-A solutions. The prediction of $Q_{P_1}^{\tau\mu}$ observable for all class-A solutions are consistent with the SM. The SM value of observable $Q_{P_2}^{\tau\mu}$ is ~ 0.35 . An enhancement of 10% is possible due to scenario S-V whereas $Q_{P_2}^{\tau\mu}$ for other class-A solutions are consistent with the SM prediction. The SM prediction of $Q_{P_3}^{\tau\mu}$ is negligibly small, $\sim 10^{-3}$. Therefore this observable can be measured only if any new physics contributions can provide a very large enhancement. However, as can be

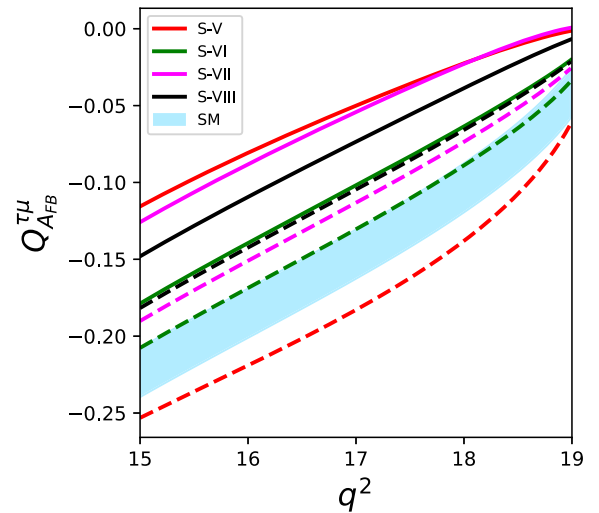


FIG. 2. Plot for the q^2 distribution in the SM as well as for several class-A new physics solutions for the $\tau - \mu$ lepton-flavor difference observable, the $Q^{\tau\mu}$ observable, for the forward backward asymmetry A_{FB} . The light blue band is due to theoretical uncertainties. The thick and dotted lines represent maximum deviation from the SM for each new physics solutions.

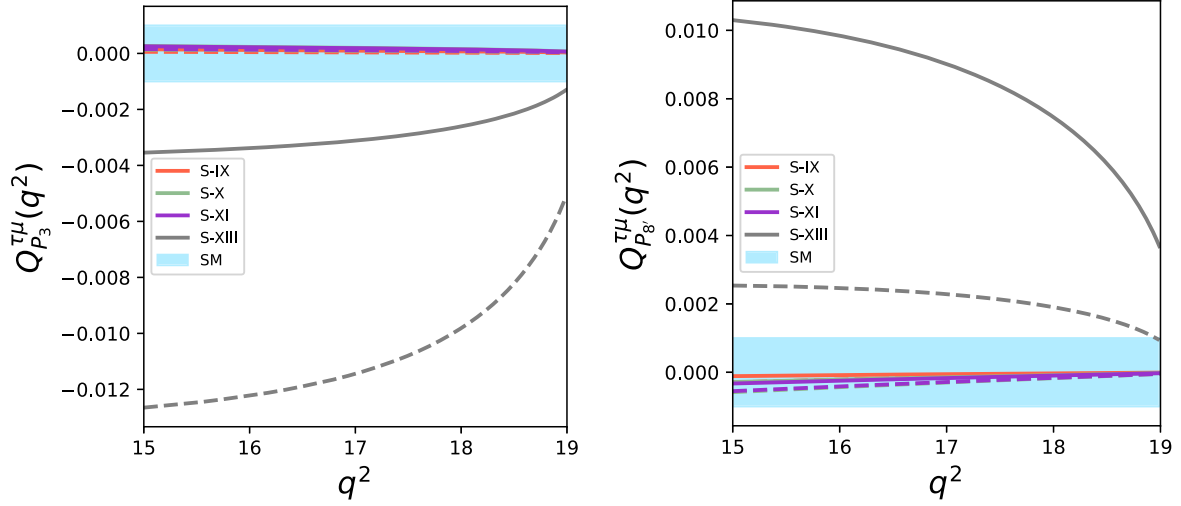


FIG. 3. Plots for the q^2 distribution in the SM as well as for class-B new physics scenarios for the $\tau - \mu$ lepton-flavor difference observables, the $Q^{\tau\mu}$ observables, for optimized observables P_3 and P'_8 . The light blue band is due to theoretical uncertainties. The thick and dotted lines represent maximum deviation from the SM for each new physics solutions.

seen from Table III, none of the class-A new physics scenarios can effectuate any meaningful enhancement in the value of $Q^{\tau\mu}_{P_3}$. The same is true for the $Q^{\tau\mu}_{P'_8}$ observable.

The SM prediction of $Q^{\tau\mu}_{P'_4}$ is ~ -0.01 . None of the class-A new physics solutions can generate any useful deviation from the SM. The observable $Q^{\tau\mu}_{P'_5}$ is predicted to be ~ -0.5 in the SM. None of the class-A scenarios show interesting results for $Q^{\tau\mu}_{P'_5}$ observable. The SM prediction of $Q^{\tau\mu}_{P'_6}$ is 0.00 ± 0.06 which remains almost the same for all class-A new physics solutions. Thus we see that none of the class-A solutions can provide any noticeable deviation from the SM in any of the $Q^{\tau\mu}_{P'_i}$ observables.

The situation, however, seems to be encouraging for class-B solutions, in particular the S-XIII solution. As can be seen from Table III, the S-XIII solution can provide large deviations from the SM in a number of $Q^{\tau\mu}_{P'_i}$ observables. For $Q^{\tau\mu}_{P'_1}$ observable, a threefold deviation from SM is

possible for S-XIII solution. For $Q^{\tau\mu}_{P'_2}$ observable, all solutions cannot dispense any illustrious difference. A tenfold enhancement in the magnitude of $Q^{\tau\mu}_{P'_3}$ is allowed for the S-XIII solution. All other solutions predict SM-like scenario for this observable.

The $Q^{\tau\mu}_{P'_i}$ observables are predicted to be close to their SM values for all class-B solutions. A threefold enhancement in the magnitude of $Q^{\tau\mu}_{P'_4}$ is allowed for the S-XIII solution. The deviation is negligible for other solutions. The S-XIII solution can effectuate an order of magnitude enhancement in the magnitude of $Q^{\tau\mu}_{P'_8}$ observable. Similar features are also delineated in the q^2 graphs (Fig. 3) of these $Q^{\tau\mu}$ observables. Thus we see that $Q^{\tau\mu}_{P'_i}$ observables can be useful in discriminating between the class-A and class-B scenarios. Any propitious deviation in these observables can only be due to class-B solutions, particularly the S-XIII solution.

TABLE IV. Results for the q^2 bin [15–19] GeV² in the SM as well as for several new physics scenarios for the $\tau - \mu$ lepton-flavor ratio observables, the $R^{\tau\mu}$ observables, the longitudinal fraction f_L , for the forward-backward asymmetry A_{FB} , and several angular observables $P_i^{(\prime)}$. Here we do not consider $R_{P_3}^{\tau\mu}$, $R_{P'_6}^{\tau\mu}$ and $R_{P'_8}^{\tau\mu}$ ratios as they have large errors due to zero crossing.

Observable	SM	S-V	S-VI	S-VII	S-VIII	S-IX	S-X	S-XI	S-XIII
$R_{K^*}^{\tau\mu}$	0.41 ± 0.01	(0.37, 0.67)	(0.39, 0.46)	(0.34, 0.40)	(0.34, 0.39)	(0.43, 0.49)	(0.45, 0.51)	(0.46, 0.51)	(0.48, 0.60)
$R_{f_L}^{\tau\mu}$	0.30 ± 0.01	(0.25, 0.31)	(0.31, 0.34)	(0.33, 0.36)	(0.34, 0.37)	(0.28, 0.30)	(0.28, 0.29)	(0.29, 0.29)	(0.28, 0.31)
$R_{A_{\text{FB}}}^{\tau\mu}$	0.58 ± 0.02	(0.49, 0.77)	(0.61, 0.67)	(0.65, 0.79)	(0.67, 0.74)	(0.56, 0.59)	(0.57, 0.61)	(0.59, 0.62)	(0.51, 0.62)
$R_{P_1}^{\tau\mu}$	1.05 ± 0.01	(1.06, 1.06)	(1.06, 1.06)	(1.06, 1.06)	(1.06, 1.06)	(1.06, 1.06)	(1.06, 1.06)	(1.06, 1.09)	(1.09, 1.28)
$R_{P_2}^{\tau\mu}$	1.94 ± 0.01	(1.92, 2.52)	(1.95, 1.97)	(1.96, 2.15)	(1.94, 1.98)	(1.94, 1.95)	(1.97, 2.06)	(2.01, 2.09)	(1.83, 2.06)
$R_{P'_4}^{\tau\mu}$	1.012 ± 0.001	(1.01, 1.01)	(1.01, 1.01)	(1.01, 1.01)	(1.01, 1.01)	(1.01, 1.01)	(1.01, 1.01)	(1.01, 1.02)	(1.02, 1.05)
$R_{P'_5}^{\tau\mu}$	1.93 ± 0.01	(1.91, 2.47)	(1.94, 1.96)	(1.95, 2.13)	(1.93, 1.96)	(1.93, 1.94)	(1.96, 2.03)	(1.98, 2.06)	(1.76, 2.02)

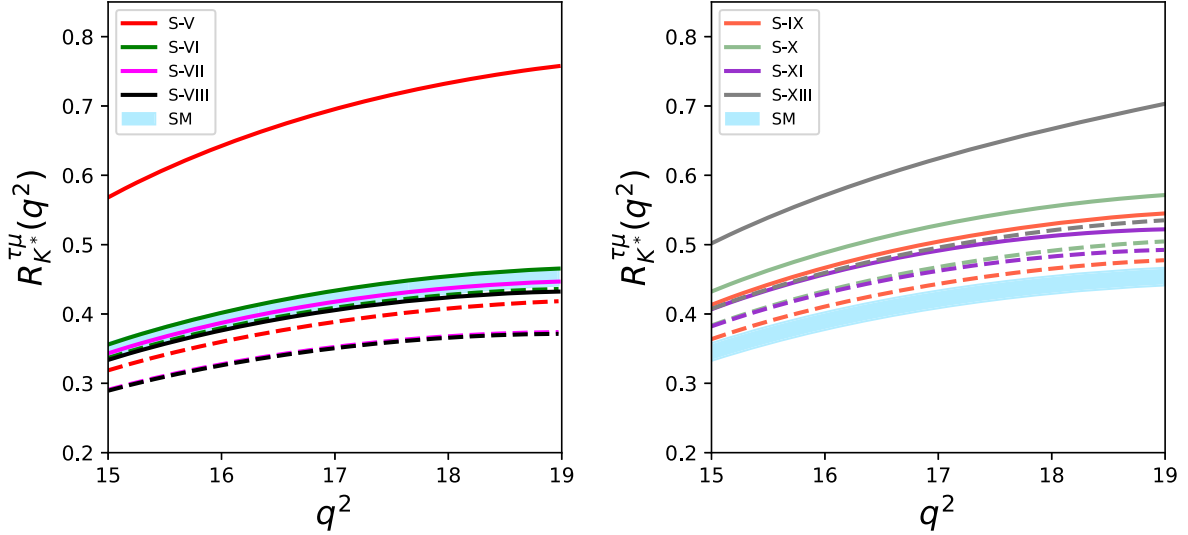


FIG. 4. Plots for the q^2 distribution in the SM as well as for several new physics solutions for the $\tau - \mu$ LFU ratio, the $R^{\tau\mu}$ observable, for the branching fraction. The left and right panels correspond to the predictions for class-A and class-B solutions, respectively. The light blue band is due to theoretical uncertainties. The thick and dotted lines represent maximum deviation from the SM for each new physics solutions.

Finally, we consider $\tau - \mu$ lepton-flavor ratios of the branching fractions, the longitudinal fractions, the forward backward asymmetries and the $P_i^{(\prime)}$ angular observables in $B \rightarrow K^* \ell \ell$ decay. The prediction for these observables in the SM as well as for favored new physics solutions belonging to class-A as well as class-B scenarios are given in Table IV.

The SM prediction of $R_{K^*}^{\tau\mu}$ is ~ 0.4 . It is apparent from Table IV that amongst the class-A new physics solutions, the S-V solution can engender largest enhancement in $R_{K^*}^{\tau\mu}$, by 60%, from the SM. The scenarios S-VII and S-VIII can suppress the value of $R_{K^*}^{\tau\mu}$, $\sim 15\%$ below the SM. These features are also articulated in the q^2 distribution of $R_{K^*}^{\tau\mu}$ which is depicted in the left panel of Fig. 4.

The class-B solutions can also relinquish large enhancements from the SM value. The largest enhancement is allowed for the S-XIII solution. This can enhance $R_{K^*}^{\tau\mu}$ by $\sim 40\%$. The S-IX, S-X, and S-XI solutions can also induce enhancement in $R_{K^*}^{\tau\mu}$. However these enhancements cannot exceed by more than $\sim 20\%$. Further, it can be espied from the right panel of Fig. 4 that none of the class-B solutions can lead to suppression in $R_{K^*}^{\tau\mu}$ below the SM value.

The SM prediction of $\tau - \mu$ flavor ratio of the longitudinal polarization asymmetries, $R_{f_L}^{\tau\mu}$, is ~ 0.3 . None of the class-A new physics scenarios, except S-V, can provide any meaningful suppression in its value. Even for S-V, the suppression can only be up to $\sim 15\%$. The new physics solution S-VII and S-VIII can ameliorate $R_{f_L}^{\tau\mu}$ by $\sim 20\%$ above the SM. Further, none of the class-B solutions can invoke any divergence from the SM value of $R_{f_L}^{\tau\mu}$.

Within the SM, the $\tau - \mu$ flavor ratio of the forward backward asymmetries, $R_{A_{FB}}^{\tau\mu}$, attains a value of ~ 0.6 . It should be noted that this ratio for $\mu - e$ observable, $R_{A_{FB}}^{\mu,e}$, in the $[1, 6]\text{GeV}^2$ region is not a good observable to probe new physics due to large errors in its SM prediction. This is due to the fact that the q^2 distribution of A_{FB} exhibits a zero crossing in this bin. For $R_{A_{FB}}^{\tau\mu}$, the relevant q^2 bin is $[15, 19]\text{GeV}^2$ for which there is no zero-crossing.

Amongst all class-A solutions, the S-V and S-VII solutions can provide largest enhancement in $R_{A_{FB}}^{\tau\mu}$. This is apparent from the left panel of Fig. 5. The enhancement can be up to 30%. None of the class-A new physics solutions can deplete $R_{A_{FB}}^{\tau\mu}$, except S-V which can induce $\sim 15\%$ depletion. Further, none of the class-B solutions can render large deviations from the SM.

We now consider $\tau - \mu$ flavor ratio of the optimized angular observables in $B \rightarrow K^* \ell \ell$ decay. The flavor ratio $R_{P_1}^{\tau\mu}$ is predicted to be ~ 1 in the SM. None of the class-A new physics solutions can provide any useful deviation from the SM. The same is true for the $R_{P_4}^{\tau\mu}$ observable for which the SM prediction is close to unity and all class-A new physics scenarios fail to provide any impact. The status remains the same for the $R_{P_4}^{\tau\mu}$ observable for class-B solutions, i.e., none of the class-B solutions can provide any visible deviation from the SM. However, as seen from the right panel of Fig. 5, for $R_{P_1}^{\tau\mu}$ observable, the S-XIII solution can invoke $\sim 20\%$ boost over the SM value.

The flavor ratio $R_{P_2}^{\tau\mu}$ is predicted to be ~ 2 in the SM. For class-A, the S-V scenario can provide 30% enhancement over the SM value. Apart from S-V, the S-VII scenario can

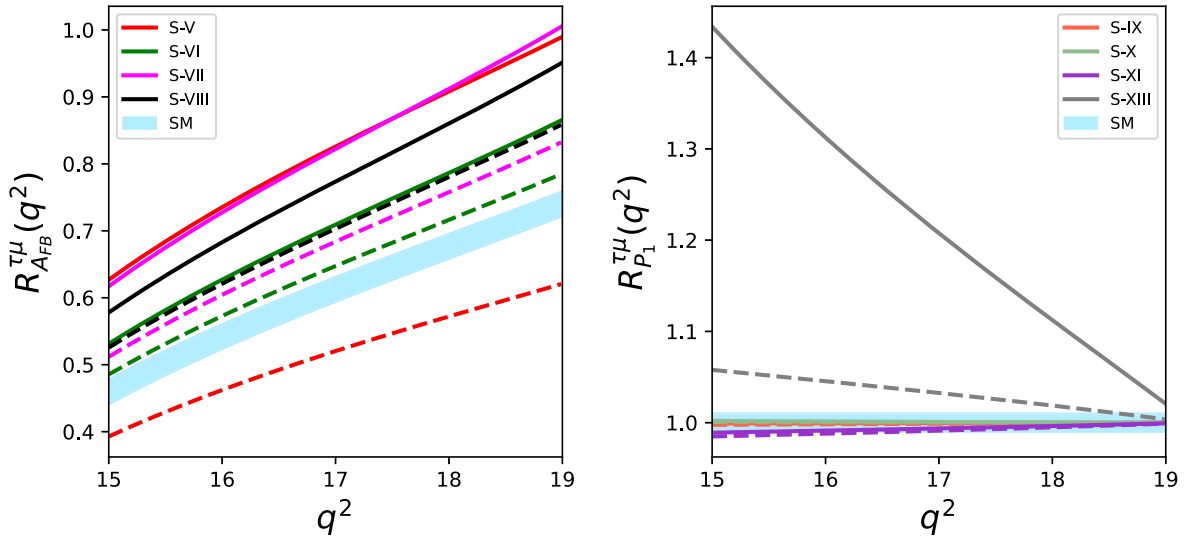


FIG. 5. Plots for the q^2 distribution in the SM as well as for several new physics solutions for the $\tau - \mu$ LFU ratio, the $R^{\tau\mu}$ observables. The left and right panels correspond to the predictions for $R^{\tau\mu}_{A_{FB}}$ (class-A solutions) and $R^{\tau\mu}_{P'_1}$ (class-B solutions), respectively. The light blue band is due to theoretical uncertainties. The thick and dotted lines represent maximum deviation from the SM for each new physics solutions.

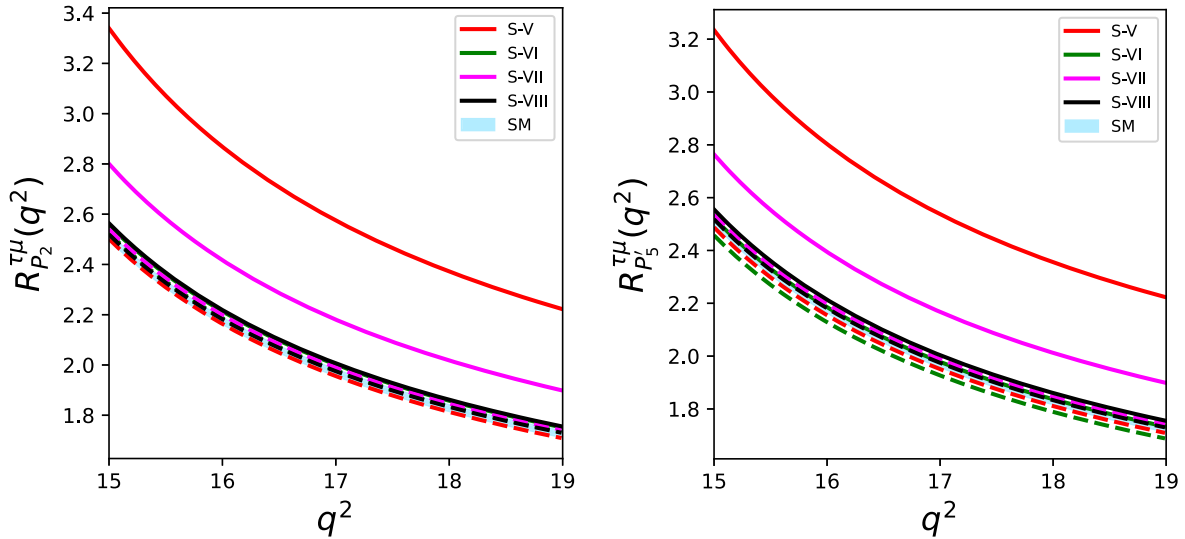


FIG. 6. Plots for the q^2 distribution in the SM as well as for several class-A new physics scenarios for the $\tau - \mu$ LFU ratios, the $R^{\tau\mu}$ observables, for the optimized observables P_2 (left panel) and P'_5 (right panel). The light blue band is due to theoretical uncertainties. The thick and dotted lines represent maximum deviation from the SM for each new physics solutions.

also enhance $R^{\tau\mu}_{P_2}$ above the SM value, the enhancement can only be up to $\sim 10\%$. These features are reflected in the q^2 plot of $R^{\tau\mu}_{P_2}$, the left panel of Fig. 6. None of the class-B solutions can generate large new physics effects in $R^{\tau\mu}_{P_2}$ observable. This is evident from Table IV. The results are almost the same for the $R^{\tau\mu}_{P'_5}$ observable. Within the SM, this observable is predicted to be ~ 2 . For class-A solutions, the

largest enhancement from the SM is provided by the S-V solution, $\sim 25\%$, as can be seen from the right panel of Fig. 6. The scenario S-VII can provide enhancement but only up to $\sim 10\%$. The class-B solutions fail to generate any observable impact on the $R^{\tau\mu}_{P'_5}$ observable except S-XIII solution which can induce marginal depletion in $R^{\tau\mu}_{P'_5}$, up to $\sim 10\%$.

Thus we see that the current data in $b \rightarrow s\mu^+\mu^-$ sector allows for large deviations in a number of observables related to the decay of $B \rightarrow K^*\tau^+\tau^-$. These observables will be particularly interesting in hunting for violation of lepton-flavor universality in $\mu - \tau$ sector. However, the situation is not so encouraging from the experimental front due to presence of multiple neutrinos in the final state. Therefore, in order to utilize the potential of $B \rightarrow K^*\tau^+\tau^-$ decay, a significant improvement in the current τ reconstruction techniques would be required.

V. CONCLUSIONS

We study the impact of current $b \rightarrow s\ell^+\ell^-$ ($\ell = e, \mu$) measurements on several observables in the decay of $B \rightarrow K^*\tau^+\tau^-$ under the assumption that the possible new physics contributions to $b \rightarrow s\ell^+\ell^-$ can have both universal as well as nonuniversal couplings to leptons. The analysis is performed in a model agnostic way using the language of effective field theory. The primary goal is to identify observables where large new physics effects are allowed by scenarios which provide a good fit to all $b \rightarrow s\ell\ell$ data. We also intend to discriminate between various new physics solutions which are classified in two categories: solutions having universal C_9 couplings and solutions with universal C_{10} or C'_{10} couplings. We denote them as class-A and class-B scenarios, respectively. In our analysis, we consider a number of observables related to $B \rightarrow K^*\tau^+\tau^-$. These include the branching fraction, the K^* longitudinal fraction f_L , the tau forward backward asymmetry A_{FB} as well as optimized angular observables $P_{1,2,3}$ and $P'_{4,5,6,8}$. We then construct $\tau - \mu$ LFUV difference (ratio) observables by taking differences (ratios) of branching fractions, f_L 's, A_{FB} 's and $P_i^{(\prime)}$'s of $B \rightarrow K^*\tau^+\tau^-$ and $B \rightarrow K^*\mu^+\mu^-$ decays.

For τ observables, i.e., for observables related only to $B \rightarrow K^*\tau^+\tau^-$ decay, we observe the following:

- (i) None of the allowed solutions can generate notable enhancement in the branching fraction of $B \rightarrow K^*\tau^+\tau^-$ decay. In fact, new physics solutions S-VII $\equiv (C_{9\mu}^V, C_9^U)$ and S-VIII $\equiv (C_{9\mu}^V = -C_{10\mu}^V, C_9^U)$ belonging to the class-A category can induce suppression up to $\sim 25\%$ as compared to the SM. No notable depletion in branching fraction is possible for any of the class-B new physics solutions.
- (ii) The K^* longitudinal fraction f_L and the tau forward backward asymmetry A_{FB} are predicted to be close to their SM values for all allowed solutions.
- (iii) No noticeable new physics effects are allowed in any of the optimized angular observables for all new physics solutions.

The results for $\tau - \mu$ LFUV difference observables, $Q^{\tau\mu}$ can be summarized as follows:

- (i) A twofold enhancement in $Q_{A_{\text{FB}}}^{\tau\mu}$ is allowed for S-V $\equiv (C_{9\mu}^V, C_{10\mu}^V, C_9^U = C_{10}^U)$ and S-VII solutions. None of the class-B solutions can induce any meaningful enhancement.
- (ii) A new physics solution, S-XIII $\equiv (C_{9\mu}^V, C_{9\mu}^{\prime V}, C_{10}^U, C_{10}^{\prime U})$ belonging to the class-B scenario can provide an order of magnitude enhancement in the absolute values of $Q_{P_3}^{\tau\mu}$ and $Q_{P_8}^{\tau\mu}$ observables whereas an enhancement up to threefold is allowed for $Q_{P_1}^{\tau\mu}$ and $Q_{P_4}^{\tau\mu}$ observables. None of the class-A solutions can provide any noticeable deviation from the SM in any of the $Q_{P_i^{(\prime)}}^{\tau\mu}$ observables.

Finally, we analyze $\tau - \mu$ LFUV ratio observables, $R^{\tau\mu}$. Our main findings are as follows:

- (i) The ratio of branching fractions of $B \rightarrow K^*\tau^+\tau^-$ and $B \rightarrow K^*\mu^+\mu^-$ can be enhanced up to 40%–50% over the SM value. This enhancement is possible for S-V as well as S-XIII solutions.
- (ii) The S-V and S-VII solutions can lead to more than 25% enhancement in $R_{A_{\text{FB}}}^{\tau\mu}$ over the SM value. No class-B solutions can induce large new physics effects in this observable.
- (iii) Amongst the flavor ratio of optimized observables, $R_{P_2}^{\tau\mu}$ and $R_{P_5}^{\tau\mu}$ can show maximum deviation, up to 25%, from the SM. This deviation is possible for new physics scenario S-V. For other ratios, only marginal deviation is allowed.

Therefore, in the considered framework, the current $b \rightarrow s\mu^+\mu^-$ data does allow for large new physics effects in a number of $B \rightarrow K^*\tau^+\tau^-$ observables. These effects range from 20%–30% up to an order of magnitude above the SM level. Hence $B \rightarrow K^*\tau^+\tau^-$ decay mode has immense potential to probe physics beyond SM, particularly by complementing the quest for new physics signatures in $b \rightarrow s\mu^+\mu^-$ sector.

ACKNOWLEDGMENTS

I would like to thank David London for his helpful advice and useful comments on the project. I also thank Shireen Gangal for fruitful discussions. I am also thankful to Ashutosh Kumar Alok for his useful suggestions and discussions along with corrections on the manuscript and Arindam Mandal for critical reading of the manuscript.

APPENDIX: ANGULAR COEFFICIENTS

The twelve q^2 dependent angular coefficients $I_i^{(a)}$ in Eq. (6) can be expressed in terms of transversity amplitudes which are given by [74]

$$\begin{aligned}
I_1^s &= \frac{(2 + \beta_\ell^2)}{4} \left[|A_\perp^L|^2 + |A_\parallel^L|^2 + (L \rightarrow R) \right] + \frac{4m_\ell^2}{q^2} \text{Re} \left(A_\perp^L A_\perp^{R*} + A_\parallel^L A_\parallel^{R*} \right), \\
I_1^c &= |A_0^L|^2 + |A_0^R|^2 + \frac{4m_\ell^2}{q^2} \left[|A_t|^2 + 2\text{Re}(A_0^L A_0^{R*}) \right] + \beta_\ell^2 |A_S|^2, \\
I_2^s &= \frac{\beta_\ell^2}{4} \left[|A_\perp^L|^2 + |A_\parallel^L|^2 + (L \rightarrow R) \right], \\
I_2^c &= -\beta_\ell^2 \left[|A_0^L|^2 + |A_0^R|^2 \right], \\
I_3 &= \frac{\beta_\ell^2}{2} \left[|A_\perp^L|^2 - |A_\parallel^L|^2 + (L \rightarrow R) \right], \\
I_4 &= \frac{\beta_\ell^2}{\sqrt{2}} \left[\text{Re}(A_0^L A_\parallel^{L*}) + (L \rightarrow R) \right], \\
I_5/\sqrt{2}\beta_\ell &= \text{Re}(A_0^L A_\perp^{L*}) - (L \rightarrow R) - \frac{m_\ell}{\sqrt{q^2}} \text{Re}(A_\parallel^L A_S^* + A_\parallel^R A_S^*), \\
I_6^s &= 2\beta_\ell \left[\text{Re}(A_\parallel^L A_\perp^{L*}) - (L \rightarrow R) \right], \\
I_6^c &= 4\beta_\ell \frac{m_\mu}{\sqrt{q^2}} \text{Re}[A_0^L A_S^* + (L \rightarrow R)], \\
I_7/\sqrt{2}\beta_\ell &= \text{Im}(A_0^L A_\parallel^{L*}) - (L \rightarrow R) + \frac{m_\mu}{\sqrt{q^2}} \text{Im}(A_\perp^L A_S^* + A_\perp^R A_S^*), \\
I_8 &= \frac{\beta_\ell^2}{\sqrt{2}} \left[\text{Im}(A_0^L A_\perp^{L*}) + (L \rightarrow R) \right], \\
I_9 &= \beta_\ell^2 \left[\text{Im}(A_\parallel^{L*} A_\perp^L) + (L \rightarrow R) \right]. \tag{A1}
\end{aligned}$$

The expression of transversity amplitudes which are written in terms of form factors $V(q^2)$, $A_{0,1,2}(q^2)$, and $T_{1,2,3}(q^2)$ can be found in Ref. [70].

-
- | | |
|---|---|
| [1] D. London and J. Matias, <i>Annu. Rev. Nucl. Part. Sci.</i> 72 , 37 (2022). | [9] ATLAS Collaboration, Report No. ATLAS-CONF-2020-049. |
| [2] R. Aaij <i>et al.</i> (LHCb Collaboration), <i>Phys. Rev. Lett.</i> 111 , 191801 (2013). | [10] M. Aaboud <i>et al.</i> (ATLAS Collaboration), <i>J. High Energy Phys.</i> 04 (2019) 098. |
| [3] R. Aaij <i>et al.</i> (LHCb Collaboration), <i>J. High Energy Phys.</i> 02 (2016) 104. | [11] A. M. Sirunyan <i>et al.</i> (CMS Collaboration), <i>J. High Energy Phys.</i> 04 (2020) 188. |
| [4] R. Aaij <i>et al.</i> (LHCb Collaboration), <i>Phys. Rev. Lett.</i> 125 , 011802 (2020). | [12] R. Aaij <i>et al.</i> (LHCb Collaboration), <i>Phys. Rev. Lett.</i> 118 , 191801 (2017). |
| [5] S. Descotes-Genon, T. Hurth, J. Matias, and J. Virto, <i>J. High Energy Phys.</i> 05 (2013) 137. | [13] W. Altmannshofer and P. Stangl, <i>Eur. Phys. J. C</i> 81 , 952 (2021). |
| [6] R. Aaij <i>et al.</i> (LHCb Collaboration), <i>J. High Energy Phys.</i> 09 (2015) 179. | [14] CMS Collaboration, Report No. CMS-PAS-BPH-21-006. |
| [7] R. Aaij <i>et al.</i> (LHCb Collaboration), <i>Phys. Rev. Lett.</i> 127 , 151801 (2021). | [15] Y. Amhis <i>et al.</i> (HFLAV Collaboration), arXiv:2206.07501 . |
| [8] R. Aaij <i>et al.</i> (LHCb Collaboration), <i>Phys. Rev. D</i> 105 , 012010 (2022). | [16] C. Bobeth, M. Gorbahn, T. Hermann, M. Misiak, E. Stamou, and M. Steinhauser, <i>Phys. Rev. Lett.</i> 112 , 101801 (2014). |
| | [17] M. Bona <i>et al.</i> (UTfit Collaboration), arXiv:2212.03894 . |

- [18] G. Hiller and F. Kruger, *Phys. Rev. D* **69**, 074020 (2004).
- [19] M. Bordone, G. Isidori, and A. Pattori, *Eur. Phys. J. C* **76**, 440 (2016).
- [20] R. Aaij *et al.* (LHCb Collaboration), *Nat. Phys.* **18**, 277 (2022).
- [21] R. Aaij *et al.* (LHCb Collaboration), *J. High Energy Phys.* **08** (2017) 055.
- [22] G. Isidori, S. Nabeebaccus, and R. Zwicky, *J. High Energy Phys.* **12** (2020) 104.
- [23] G. Isidori, D. Lancierini, S. Nabeebaccus, and R. Zwicky, *J. High Energy Phys.* **10** (2022) 146.
- [24] S. Nabeebaccus and R. Zwicky, [arXiv:2209.09585](https://arxiv.org/abs/2209.09585).
- [25] R. Aaij *et al.* (LHCb Collaboration), *Phys. Rev. Lett.* **128**, 191802 (2022).
- [26] B. Capdevila, S. Descotes-Genon, J. Matias, and J. Virto, *J. High Energy Phys.* **10** (2016) 075.
- [27] S. Wehle *et al.* (Belle Collaboration), *Phys. Rev. Lett.* **118**, 111801 (2017).
- [28] S. Descotes-Genon, J. Matias, and J. Virto, *Phys. Rev. D* **88**, 074002 (2013).
- [29] W. Altmannshofer and D. M. Straub, *Eur. Phys. J. C* **73**, 2646 (2013).
- [30] T. Hurth and F. Mahmoudi, *J. High Energy Phys.* **04** (2014) 097.
- [31] A. K. Alok, B. Bhattacharya, D. Kumar, J. Kumar, D. London, and S. U. Sankar, *Phys. Rev. D* **96**, 015034 (2017).
- [32] A. K. Alok, A. Dighe, S. Gangal, and D. Kumar, *J. High Energy Phys.* **06** (2019) 089.
- [33] A. Carvunis, F. Dettori, S. Gangal, D. Guadagnoli, and C. Normand, *J. High Energy Phys.* **12** (2021) 078.
- [34] L. S. Geng, B. Grinstein, S. Jäger, S. Y. Li, J. Martin Camalich, and R. X. Shi, *Phys. Rev. D* **104**, 035029 (2021).
- [35] M. Algueró, B. Capdevila, S. Descotes-Genon, J. Matias, and M. Novoa-Brunet, *Eur. Phys. J. C* **82**, 326 (2022).
- [36] T. Hurth, F. Mahmoudi, D. M. Santos, and S. Neshatpour, *Phys. Lett. B* **824**, 136838 (2022).
- [37] A. Angelescu, D. Bečirević, D. A. Faroughy, F. Jaffredo, and O. Sumensari, *Phys. Rev. D* **104**, 055017 (2021).
- [38] A. K. Alok, N. R. Singh Chundawat, S. Gangal, and D. Kumar, *Eur. Phys. J. C* **82**, 967 (2022).
- [39] N. R. Singh Chundawat, [arXiv:2207.10613](https://arxiv.org/abs/2207.10613).
- [40] M. Ciuchini, M. Fedele, E. Franco, A. Paul, L. Silvestrini, and M. Valli, *Eur. Phys. J. C* **83**, 64 (2023).
- [41] T. Hurth, F. Mahmoudi, D. Martinez Santos, and S. Neshatpour, [arXiv:2210.07221](https://arxiv.org/abs/2210.07221).
- [42] J. Kumar and D. London, *Phys. Rev. D* **99**, 073008 (2019).
- [43] M. Algueró, B. Capdevila, S. Descotes-Genon, P. Masjuan, and J. Matias, *Phys. Rev. D* **99**, 075017 (2019).
- [44] M. Algueró, B. Capdevila, A. Crivellin, S. Descotes-Genon, P. Masjuan, J. Matias, M. Novoa Brunet, and J. Virto, *Eur. Phys. J. C* **79**, 714 (2019).
- [45] LHCb Collaboration, [arXiv:2212.09152](https://arxiv.org/abs/2212.09152).
- [46] LHCb Collaboration, [arXiv:2212.09153](https://arxiv.org/abs/2212.09153).
- [47] M. Ciuchini, M. Fedele, E. Franco, A. Paul, L. Silvestrini, and M. Valli, [arXiv:2212.10516](https://arxiv.org/abs/2212.10516).
- [48] B. Capdevila, A. Crivellin, S. Descotes-Genon, L. Hofer, and J. Matias, *Phys. Rev. Lett.* **120**, 181802 (2018).
- [49] M. Algueró, J. Matias, B. Capdevila, and A. Crivellin, *Phys. Rev. D* **105**, 113007 (2022).
- [50] A. de Giorgi and G. Piazza, [arXiv:2211.05595](https://arxiv.org/abs/2211.05595).
- [51] E. Kou *et al.* (Belle-II Collaboration), *Prog. Theor. Exp. Phys.* **2019**, 123C01 (2019); **2020**, 029201(E) (2020).
- [52] A. Crivellin, D. Müller, and C. Wiegand, *J. High Energy Phys.* **06** (2019) 119.
- [53] C. Bobeth, A. J. Buras, A. Celis, and M. Jung, *J. High Energy Phys.* **04** (2017) 079.
- [54] A. Crivellin, C. Greub, D. Müller, and F. Saturnino, *Phys. Rev. Lett.* **122**, 011805 (2019).
- [55] A. Abdesselam *et al.* (Belle Collaboration), *Phys. Rev. Lett.* **126**, 161801 (2021).
- [56] R. Aaij *et al.* (LHCb Collaboration), *J. High Energy Phys.* **11** (2016) 047.
- [57] V. Khachatryan *et al.* (CMS Collaboration), *Phys. Lett. B* **753**, 424 (2016).
- [58] CDF Collaboration, CDF public note 10894, <https://inspirehep.net/files/4e57b65db46b7d8328b605f50325a876>.
- [59] R. Aaij *et al.* (LHCb Collaboration), *J. High Energy Phys.* **06** (2014) 133.
- [60] J. P. Lees *et al.* (BABAR Collaboration), *Phys. Rev. Lett.* **112**, 211802 (2014).
- [61] M. Aaboud *et al.* (ATLAS Collaboration), *J. High Energy Phys.* **10** (2018) 047.
- [62] A. M. Sirunyan *et al.* (CMS Collaboration), *Phys. Lett. B* **781**, 517 (2018).
- [63] R. Aaij *et al.* (LHCb Collaboration), *Phys. Rev. Lett.* **126**, 161802 (2021).
- [64] R. Aaij *et al.* (LHCb Collaboration), *J. High Energy Phys.* **11** (2021) 043.
- [65] R. Aaij *et al.* (LHCb Collaboration), *J. High Energy Phys.* **05** (2013) 159.
- [66] R. Aaij *et al.* (LHCb Collaboration), *Phys. Rev. Lett.* **113**, 151601 (2014).
- [67] R. Aaij *et al.* (LHCb Collaboration), *J. High Energy Phys.* **04** (2015) 064.
- [68] F. James and M. Roos, *Comput. Phys. Commun.* **10**, 343 (1975).
- [69] D. M. Straub, [arXiv:1810.08132](https://arxiv.org/abs/1810.08132).
- [70] A. Bharucha, D. M. Straub, and R. Zwicky, *J. High Energy Phys.* **08** (2016) 098.
- [71] N. Gubernari, A. Kokulu, and D. van Dyk, *J. High Energy Phys.* **01** (2019) 150.
- [72] R. Aaij *et al.* (LHCb Collaboration), *J. High Energy Phys.* **08** (2013) 131.
- [73] F. Kruger, L. M. Sehgal, N. Sinha, and R. Sinha, *Phys. Rev. D* **61**, 114028 (2000); **63**, 019901(E) (2001).
- [74] W. Altmannshofer, P. Ball, A. Bharucha, A. J. Buras, D. M. Straub, and M. Wick, *J. High Energy Phys.* **01** (2009) 019.
- [75] J. Gratex, M. Hopfer, and R. Zwicky, *Phys. Rev. D* **93**, 054008 (2016).
- [76] C. Bobeth, G. Hiller, and G. Piranishvili, *J. High Energy Phys.* **07** (2008) 106.
- [77] F. Kruger and J. Matias, *Phys. Rev. D* **71**, 094009 (2005).
- [78] U. Egede, T. Hurth, J. Matias, M. Ramon, and W. Reece, *J. High Energy Phys.* **11** (2008) 032.
- [79] C. Bobeth, G. Hiller, and D. van Dyk, *J. High Energy Phys.* **07** (2011) 067.
- [80] D. Becirevic and E. Schneider, *Nucl. Phys.* **B854**, 321 (2012).

- [81] J. Matias, F. Mescia, M. Ramon, and J. Virto, *J. High Energy Phys.* **04** (2012) 104.
- [82] S. Descotes-Genon, T. Hurth, J. Matias, and J. Virto, *J. High Energy Phys.* **05** (2013) 137.
- [83] A. Khodjamirian, T. Mannel, A. A. Pivovarov, and Y. M. Wang, *J. High Energy Phys.* **09** (2010) 089.
- [84] M. Beneke, T. Feldmann, and D. Seidel, *Nucl. Phys.* **B612**, 25 (2001).
- [85] S. Descotes-Genon, L. Hofer, J. Matias, and J. Virto, *J. High Energy Phys.* **12** (2014) 125.
- [86] B. Capdevila, S. Descotes-Genon, L. Hofer, and J. Matias, *J. High Energy Phys.* **04** (2017) 016.
- [87] C. Bobeth, M. Chrzaszcz, D. van Dyk, and J. Virto, *Eur. Phys. J. C* **78**, 451 (2018).
- [88] T. Blake, U. Egede, P. Owen, K. A. Petridis, and G. Pomery, *Eur. Phys. J. C* **78**, 453 (2018).
- [89] N. Gubernari, D. van Dyk, and J. Virto, *J. High Energy Phys.* **02** (2021) 088.
- [90] R. R. Horgan, Z. Liu, S. Meinel, and M. Wingate, *Phys. Rev. D* **89**, 094501 (2014).
- [91] J. Flynn, A. Jüttner, T. Kawanai, E. Lizarazo, and O. Witzel, *Proc. Sci. LATTICE2015* (**2016**) 345 [arXiv:1511.06622].
- [92] W. Altmannshofer and D. M. Straub, *Eur. Phys. J. C* **75**, 382 (2015).
- [93] S. Jäger and J. Martin Camalich, *Phys. Rev. D* **93**, 014028 (2016).
- [94] W. Altmannshofer and I. Yavin, *Phys. Rev. D* **92**, 075022 (2015).